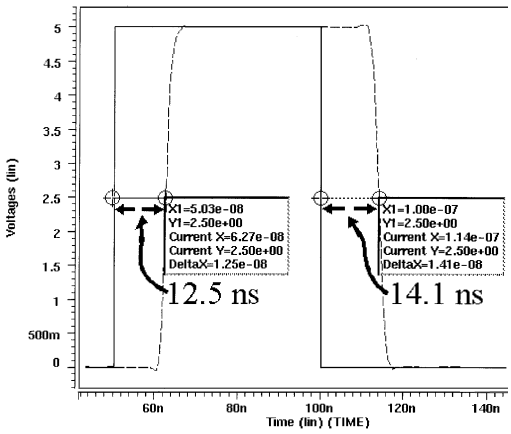

Fig. 4. Simulation result using LPE netlist.

produced. HSPICE is then used to resimulate the delay of this LPE extracted netlist. The simulation result is shown in Fig. 4. The maximum rise delay is 12.5 ns while the maximum fall delay is 14.1 ns. It gives a reasonable explanation that parasitic effects are to be blamed for the degradation of the speed performance.

VII. Conclusion

Several dynamic CMOS comparators are proposed with a number of advantages. The transistor count is much less than that of the other similar designs, and the total area size is less than that of the prior comparators. Furthermore, the noise immunity is better than the prior comparators. Although it has high fan in, the number of series transistors in the N-transistor evaluation block is two, which in turns reduce the pull down delay.

References

[1] C.-C. Wang, C.-F. Wu, S.-H. Chen, and C.-H. Kao, "In sawing lanes multilevel BIST for known good dies of LCD drivers," *Electron. Lett.*, vol. 35, no. 84, pp. 1543–154, 1999.

[2] L. T. Clark and G. F. Taylor, "High fan-in circuit design," *IEEE J. Solid-State Circuits*, vol. 31, pp. 91–96, Jan. 1996.

[3] V. Fried and S. Liu, "Dynamic logic CMOS circuit," *IEEE J. Solid-State Circuits*, vol. SC-19, pp. 263–266, Apr. 1984.

[4] N. F. Gonclaves and H. J. DeMan, "NORA: A racefree dynamic CMOS technique for pipelined logic structures," *IEEE J. Solid-State Circuits*, vol. SC-18, pp. 261–266, June 1983.

[5] N. H. E. Weste and K. Eshraghian, *Principle of CMOS VLSI Design a System Perspective*. Reading, MA: Addison Wesley, 1993.

[6] C.-F. Wu, C.-C. Wang, R.-T. Hwang, and C.-H. Kao, "IDDQ testable configuration for PLA's by transformation into inverters," in *Proc. Int. Symp. Integrated Circuit Technology Systems and Applications*, Sept. 1997, pp. 398–401.

[7] A. J. van de Goor, *Testing Semiconductor Memories Theory and Practice*. New York: Wiley, 1994.

[8] C.-C. Wang, C.-F. Wu, and K.-C. Tsai, "A 1.0 GHz 64-bit high-speed comparator using ANT dynamic logic with two-phase clocking," in *Proc. Inst . Elect. Eng.— Comput., Digital Tech.*, vol. 145, 1998, pp. 433–436.

[9] M. Afghahi, "A robust single phase clocking for low power, high-speed VLSI application," *IEEE J. Solid-State Circuits*, vol. 31, pp. 247–253, Feb. 1996.

[10] R. X. Gu and M. I. Elmasry, "All-N-logic high-speed true-single-phase dynamic CMOS logic," *IEEE J. Solid-State Circuits*, vol. 31, pp. 221–229, Feb. 1996.

Analysis of Three-Phase Rectifiers With Constant-Voltage Loads

Vahe Caliskan, David J. Perreault, Thomas M. Jahns, and John G. Kassakian

***Abstract*—This brief presents a quantitative analysis of the operating characteristics of three-phase diode bridge rectifiers with ac-side reactance and constant-voltage loads. We focus on the case where the ac-side currents vary continuously (continuous ac-side conduction mode). This operating mode is of particular importance in alternators and generators, for example. Simple approximate expressions are derived for the line and output current characteristics as well as the input power factor. Expressions describing the necessary operating conditions for continuous ac-side conduction are also developed. The derived analytical expressions are applied to practical examples and both simulations and experimental results are utilized to validate the analytical results. It is shown that the derived expressions are far more accurate than calculations based on traditional constant-current models.**

***Index Terms*—Alternator, commutation, converter, generator, load matching, load regulation, .**

I. Introduction

In a number of power-electronics applications, one encounters a three-phase bridge rectifier that is supplied from an inductive ac source and drives a constant-voltage load,[1] as illustrated in Fig. 1. For example, this often occurs in battery-charger/power-supply systems, such as employed in automotive and aerospace applications. The three-phase source with series inductance represents the alternator back emf and synchronous inductance, while the constant-voltage load represents the battery and system loads. A similar situation can occur when a transformer-driven rectifier is loaded with a capacitive output filter when the dc-side impedance is much lower than the ac-side impedance (as may occur during heavy- or over-load conditions). Here, the ac-side inductance is due to line, filter, and transformer leakage reactances, while the dc-side filter and load act as a constant-voltage load. In all such applications, the rectifier input and output currents are functions of the system voltage levels and the ac-side reactance.

While one might expect that analytical models for the operational characteristics of the system of Fig. 1 would be readily available in the literature, this appears not to be the case. The behavior of single-phase diode rectifier circuits with ac-side impedance and capacitive loading have been treated in the work of Schade and others [2]–[7]. Most treatments of three-phase rectifier circuits only consider operation with inductive (or constant-current) loading of the rectifier (e.g., [1], [8], and

Manuscript received July 12, 2000; revised December 14, 2000 amd March 18, 2003. This work was supported by the member companies of the MIT/Industry Consortium on Advanced Automotive Electrical/Electronic Components and Systems. This paper was recommended by Associate Editor D. Czarkowski.

V. Caliskan, D. J. Perreault, and J. G. Kassakian are with the Laboratory for Electromagnetic and Electronic Systems, Massachusetts Institute of Technology, Cambridge, MA 02139 USA (e-mail: vahe@mit.edu; djperrea@mit.edu; jgk@mit.edu).

T. M. Jahns is with the Department of Electrical and Computer Engineering, University of Wisconsin—Madison, Madison, WI 53706 USA (e-mail: jahns@engr.wisc.edu).

Digital Object Identifier 10.1109/TCSI.2003.816323

[1]In "constant-voltage" loads, we also include "zero-ripple-voltage" loads where the dc-side voltage (e.g., a filter capacitor voltage) may vary over time *but not substantially within an ac cycle*. In such cases, the results presented here describe the *local average* operating behavior of the system [1].

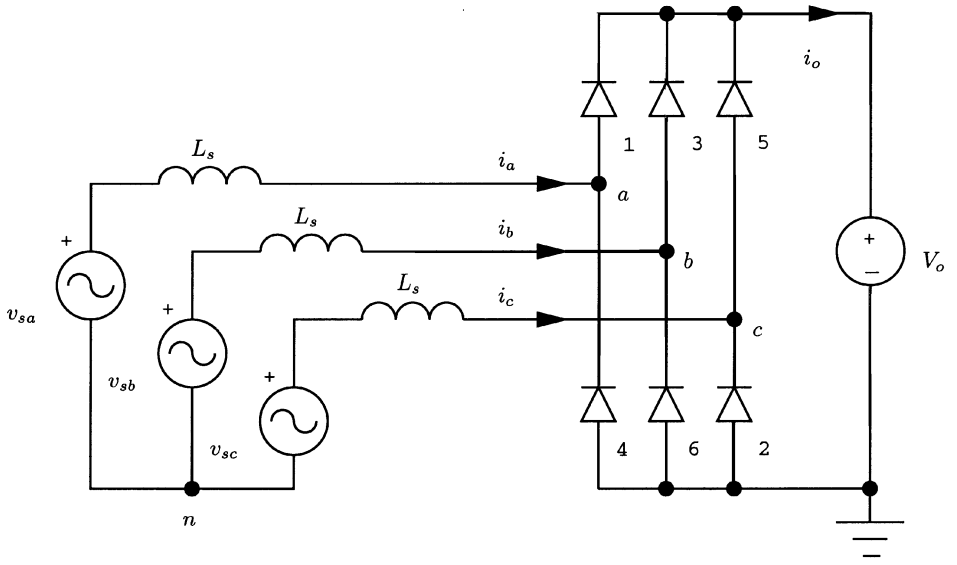

Fig. 1. Three-phase diode bridge rectifier with a constant-voltage load and ac-side reactance.

[9]). Schaefer [8] does devote a chapter to rectifiers with ac-side reactance and capacitive loading, with a primary focus on single-phase circuits and the three-phase midpoint connection circuit. The three-phase bridge rectifier is treated for a light-load (discontinuous ac-side conduction mode[2]) case, but the chapter stops short of fully analyzing the bridge rectifier in continuous ac-side conduction, noting that the analysis is complex. More recently, Grotzbach [10] evaluates operation in some discontinuous ac-side conduction modes utilizing simulation-based nomographs.

This brief presents a quantitative analysis of the operating characteristics of bridge rectifiers with ac-side reactance and constant-voltage loads in continuous ac-side conduction. Section II describes the operating characteristics of the three-phase diode bridge rectifier in this mode. Simple approximate expressions are derived for the output current characteristics as well as the input power factor. The results are also extended to the case where the ac-side impedances have a resistive component. Section III of the brief analyzes the boundary conditions for the mode of operation considered in the brief. Section IV of the brief applies these newly derived analytical expressions to a practical example, and validates the results against simulations and experimental results.

II. Three-Phase Diode Rectifier With Constant-Voltage Load

A three-phase rectifier with a constant-voltage load V_o is shown in Fig. 1. Also included are line inductances L_s in series with a balanced three-phase set of sinusoidal voltages $v_{\rm sa}$, $v_{\rm sb}$, and $v_{\rm sc}$ with magnitude V_s and angular frequency ω

$$v_{\rm sa} = V_s \sin(\omega t) \tag{1}$$
$$v_{\rm sb} = V_s \sin(\omega t - 2\pi/3) \tag{2}$$
$$v_{\rm sc} = V_s \sin(\omega t + 2\pi/3). \tag{3}$$

The diodes in the full bridge rectifier are assumed ideal except for a finite on-voltage, V_d. Assuming that the source currents i_a, i_b, and i_c vary continuously (i.e., do not stay at zero over part of the cycle), it can be shown that the line-to-ground voltages $v_{\rm ag}$, $v_{\rm bg}$, and $v_{\rm cg}$ and the neutral-to-ground voltage $v_{\rm ng}$ are given by

$$v_{\rm ag} = \frac{V_o}{2} + \left(\frac{V_o}{2} + V_d\right) \operatorname{sgn}(i_a) \tag{4}$$
$$v_{\rm bg} = \frac{V_o}{2} + \left(\frac{V_o}{2} + V_d\right) \operatorname{sgn}(i_b) \tag{5}$$
$$v_{\rm cg} = \frac{V_o}{2} + \left(\frac{V_o}{2} + V_d\right) \operatorname{sgn}(i_c) \tag{6}$$
$$v_{\rm ng} = \frac{V_o}{2} + \frac{1}{3}\left(\frac{V_o}{2} + V_d\right)[\operatorname{sgn}(i_a) + \operatorname{sgn}(i_b) + \operatorname{sgn}(i_c)] \tag{7}$$

where $\operatorname{sgn}(\cdot)$ is the signum function defined as

$$\operatorname{sgn}(x) \triangleq \begin{cases} +1, & \text{if } x > 0 \\ -1, & \text{if } x < 0 \\ 0, & \text{if } x = 0. \end{cases} \tag{8}$$

Using ground referenced voltages (4)–(7), the full bridge rectifier and constant-voltage V_o can be replaced by three line-to-neutral voltages given by

$$v_{\rm an} \triangleq v_{\rm ag} - v_{\rm ng} = \left(\frac{V_o}{2} + V_d\right) \operatorname{sgn}(i_a) - \frac{1}{3}\left(\frac{V_o}{2} + V_d\right)[\operatorname{sgn}(i_a) + \operatorname{sgn}(i_b) + \operatorname{sgn}(i_c)] \tag{9}$$
$$v_{\rm bn} \triangleq v_{\rm bg} - v_{\rm ng} = \left(\frac{V_o}{2} + V_d\right) \operatorname{sgn}(i_b) - \frac{1}{3}\left(\frac{V_o}{2} + V_d\right)[\operatorname{sgn}(i_a) + \operatorname{sgn}(i_b) + \operatorname{sgn}(i_c)] \tag{10}$$
$$v_{\rm cn} \triangleq v_{\rm cg} - v_{\rm ng} = \left(\frac{V_o}{2} + V_d\right) \operatorname{sgn}(i_c) - \frac{1}{3}\left(\frac{V_o}{2} + V_d\right)[\operatorname{sgn}(i_a) + \operatorname{sgn}(i_b) + \operatorname{sgn}(i_c)]. \tag{11}$$

We will now approximate the voltages $v_{\rm an}$, $v_{\rm bn}$, and $v_{\rm cn}$ by their fundamental components, $v_{\rm an1}$, $v_{\rm bn1}$, and $v_{\rm cn1}$, respectively. This approximation is justified for two reasons. First, since the back emf is sinusoidal, power transfer can only be achieved through the fundamental. Second, consider the shape of waveform $v_{\rm an}$, illustrated in Fig. 2 and

[2]For purposes of this brief, we define discontinuous and continuous conduction with respect to the ac line currents. That is, in continuous ac-side conduction the ac line currents vary continuously, while in discontinuous ac-side conduction they remain at zero for some part of the cycle.

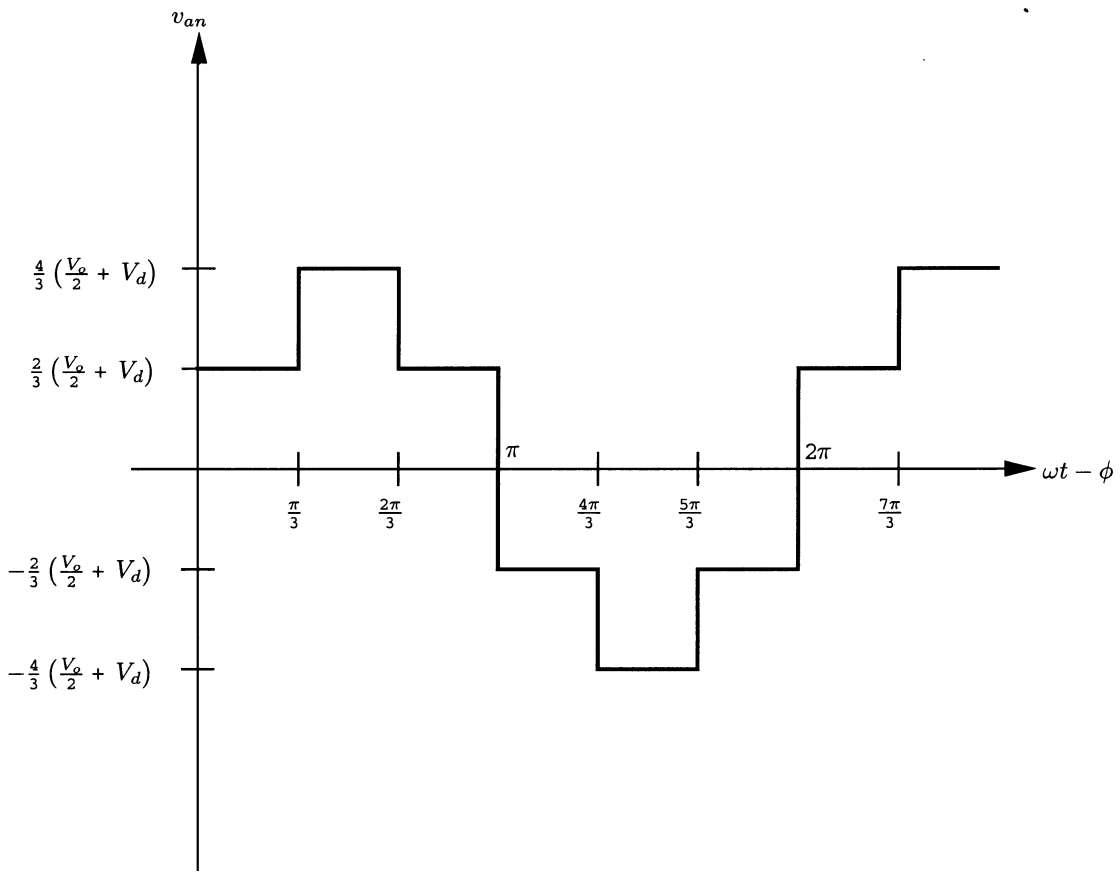

Fig. 2. Rectifier phase $\boldsymbol{a}$ line-to-neutral voltage $\boldsymbol{v}_{\rm an}$.

described by the Fourier Series magnitude coefficients

$$v_{an,k}=\begin{cases}\dfrac{4}{k\pi}\left(\dfrac{V_o}{2}+V_d\right), & \text{for } k=1,5,7,11,13,\ldots\\ 0, & \text{otherwise.}\end{cases} \tag{12}$$

The lowest harmonic is the fifth, with a magnitude of only 20% of that of the fundamental. Since the impedance of inductances L_s rises linearly with frequency, the largest harmonic *current* component that arises is also the fifth and is only 4% of that due to the fundamental. Thus, we conclude that for circuit operation and power transfer purposes $v_{\rm an}$, $v_{\rm bn}$, and $v_{\rm cn}$ are well represented by their fundamental components.

This approximation yields

$$v_{\rm an}\approx v_{\rm an\,1}=V_{o1}\sin(\omega t-\phi) \tag{13}$$
$$v_{\rm bn}\approx v_{\rm bn\,1}=V_{o1}\sin(\omega t-\phi-2\pi/3) \tag{14}$$
$$v_{\rm cn}\approx v_{\rm cn\,1}=V_{o1}\sin(\omega t-\phi+2\pi/3) \tag{15}$$

where $V_{o1}=(4)/(\pi)(V_o/2+V_d)$ and ϕ is the phase angle between each voltage source $(v_{\rm sa},v_{\rm sb},v_{\rm sc})$ and its corresponding voltage sink $(v_{\rm an\,1},v_{\rm bn\,1},v_{\rm cn\,1})$ for each phase. Given expressions (13)–(15), we can also approximate the line currents i_a,i_b, and i_c by their fundamental components i_{a1},i_{b1}, and i_{c1}, respectively. Furthermore, since we know voltages $v_{\rm an\,1},v_{\rm bn\,1}$, and $v_{\rm cn\,1}$ are in phase with their respective line currents due to the switching pattern of the rectifier, the phase currents will have the form

$$i_a\approx i_{a1}=I_{s1}\sin(\omega t-\phi) \tag{16}$$
$$i_b\approx i_{b1}=I_{s1}\sin(\omega t-\phi-2\pi/3) \tag{17}$$
$$i_c\approx i_{c1}=I_{s1}\sin(\omega t-\phi+2\pi/3) \tag{18}$$

where I_{s1} and ϕ are the magnitude and phase, respectively, of the fundamental component of the line currents yet to be determined. Since the line currents i_{a1},i_{b1}, and i_{c1} are in phase with their respective line-to-neutral voltages $v_{\rm an\,1},v_{\rm bn\,1},v_{\rm cn\,1}$, we may replace the line-neutral voltages by equivalent resistances (R) defined by

$$R\triangleq\frac{V_{o1}}{I_{s1}}. \tag{19}$$

An equivalent circuit for the simplified three-phase full bridge rectifier model is shown in Fig. 3. To determine the magnitude of the fundamental component of the line current, we only need to examine one of the phases. For example, the phasor of the line current in phase a is given by

$$\mathbf{I}_a=\frac{V_s}{\sqrt{R^2+(\omega L_s)^2}}e^{-j\tan^{-1}(\omega L_s/R)}\triangleq I_{s1}e^{-j\phi}. \tag{20}$$

Substituting the expression for I_{s1} into (19), the equivalent resistance R may now be written as

$$R\triangleq\frac{V_{o1}}{I_{s1}}=\frac{V_{o1}\sqrt{R^2+(\omega L_s)^2}}{V_s}. \tag{21}$$

Solving for R in (21) yields

$$R=\frac{\omega L_s V_{o1}}{\sqrt{{V_s}^2-{V_{o1}}^2}}. \tag{22}$$

Note that our approximation for the equivalent resistance is valid if and only if $(V_s)/(V_{o1})>1$, which we show to be true for this operating mode in Section III. Using the expression for the equivalent resistance

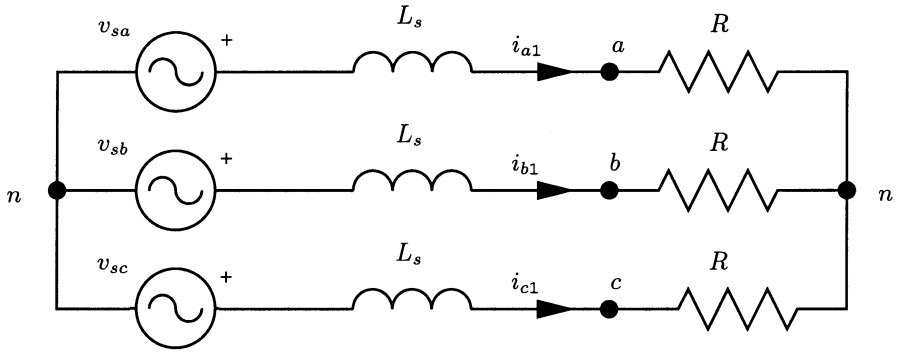

Fig. 3. Averaged model for the three-phase rectifier using equivalent resistance $\boldsymbol{R}$.

R in (22), the magnitude of the fundamental of the line current I_{s1} and the phase angle ϕ can be expressed as

$$I_{s1} = \frac{\sqrt{{V_s}^2 - {V_{o1}}^2}}{\omega L_s} = \frac{\sqrt{{V_s}^2 - \frac{16}{\pi^2}\left(\frac{V_o}{2} + V_d\right)^2}}{\omega L_s} \tag{23}$$

$$\phi = \tan^{-1}\sqrt{(V_s/V_{o1})^2 - 1} = \tan^{-1}\sqrt{\frac{\pi^2 {V_s}^2}{16\left(\frac{V_o}{2} + V_d\right)^2} - 1}. \tag{24}$$

The average output current delivered to the constant-voltage load V_o can be approximated as

$$\langle i_o \rangle \approx \frac{3}{\pi} I_{s1} = \frac{3}{\pi}\frac{\sqrt{{V_s}^2 - {V_{o1}}^2}}{\omega L_s} = \frac{3}{\pi}\frac{\sqrt{{V_s}^2 - \frac{16}{\pi^2}\left(\frac{V_o}{2} + V_d\right)^2}}{\omega L_s}. \tag{25}$$

As will be shown in Section III, distortion does not contribute significantly to the power factor in this mode. Thus, the power factor k_p may be computed using the expression for ϕ

$$k_p \approx \cos\phi = \frac{V_{o1}}{V_s} = \frac{4\left(\frac{V_o}{2} + V_d\right)}{\pi V_s}. \tag{26}$$

In our derivation of the equivalent resistance R given in (22), we included the impact of the line inductances but neglected series resistances to simplify the analysis. The inclusion of series resistance into the analysis is straightforward; however, it does complicate the expressions. For example, if we assume that each phase has a line inductance L_s and series resistance R_s associated with it, the expression for the equivalent resistance R becomes

$$R = \frac{{V_{o1}}^2 R_s + V_{o1}\sqrt{(\omega L_s)^2\left({V_s}^2 - {V_{o1}}^2\right) + R_s^2 V_s^2}}{{V_s}^2 - {V_{o1}}^2}. \tag{27}$$

Using (27), one can derive new expressions for I_{s1}, ϕ, and $\langle i_o \rangle$ which includes the series resistance R_s, as shown in (28)–(30) at bottom of the page.

III. Operating Conditions for Continuous AC-Side Conduction

To make effective use of the preceding analysis, it is important to understand the conditions for which it applies. Here we establish the range of operating conditions over which the results are applicable.

Some of the necessary conditions are implicit in Fig. 1. First, the rectifier output voltage must have very small ripple over the ac line cycle (though it may vary over much longer time scales). This means that the dc-side impedance must be much smaller than the ac-side impedances for the ripple frequencies involved. The ac-side voltages and impedances must also form a balanced three-phase set. (The ac voltages can have arbitrary triple-n harmonics and a small amount of other harmonics without greatly affecting the results).

In continuous ac-side conduction, three diodes must conduct at all times. Consider the transition that occurs when current i_a in Fig. 1 crosses zero in the positive-going direction. Prior to this transition, devices 4, 5, and 6 were conducting. As i_a reaches zero, device 4 turns off. For continuous ac-side conduction, source voltage $v_{\rm sa}$ must be large enough to immediately turn device 1 on. This requirement may be expressed as

$$v_{\rm sa}(t^+{}_{\rm cross}) + v_{\rm ng}(t^+{}_{\rm cross}) \geq V_o + V_d. \tag{31}$$

$$I_{s1} = \frac{{V_s}^2 - \frac{16}{\pi^2}\left(\frac{V_o}{2} + V_d\right)^2}{\frac{4}{\pi}\left(\frac{V_o}{2} + V_d\right)R_s + \sqrt{(\omega L_s)^2\left({V_s}^2 - \frac{16}{\pi^2}\left(\frac{V_o}{2} + V_d\right)^2\right) + R_s^2 V_s^2}} \tag{28}$$

$$\phi = \tan^{-1}\left[\frac{\omega L_s\left({V_s}^2 - \frac{16}{\pi^2}\left(\frac{V_o}{2} + V_d\right)^2\right)}{R_s {V_s}^2 + \frac{4}{\pi}\left(\frac{V_o}{2} + V_d\right)\sqrt{(\omega L_s)^2\left({V_s}^2 - \frac{16}{\pi^2}\left(\frac{V_o}{2} + V_d\right)^2\right) + R_s^2 V_s^2}}\right] \tag{29}$$

$$\langle i_o \rangle \approx \frac{3}{\pi} I_{s1} = \frac{3}{\pi}\frac{{V_s}^2 - \frac{16}{\pi^2}\left(\frac{V_o}{2} + V_d\right)^2}{\frac{4}{\pi}\left(\frac{V_o}{2} + V_d\right)R_s + \sqrt{(\omega L_s)^2\left({V_s}^2 - \frac{16}{\pi^2}\left(\frac{V_o}{2} + V_d\right)^2\right) + R_s^2 V_s^2}} \tag{30}$$

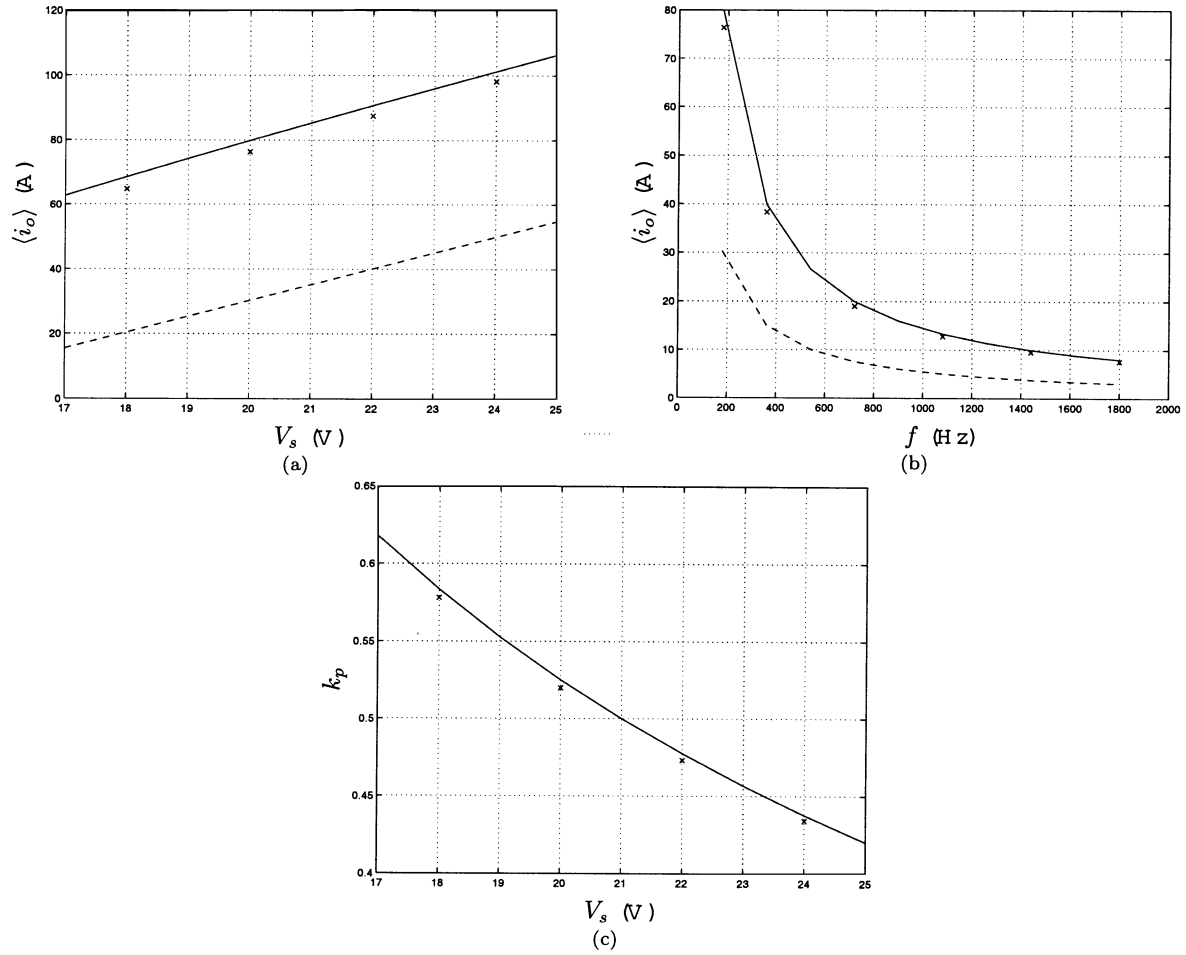

Fig. 4. Comparison of analytical calculations and simulation results. (a) $\langle \boldsymbol{i}_o \rangle$ versus $\boldsymbol{V}_s$. (b) $\langle \boldsymbol{i}_o \rangle$ versus $\boldsymbol{f}$ (solid: analytical, $\times$: simulation, dashed: classical constant-current model). (c) Power factor $\boldsymbol{k}_p$ versus $\boldsymbol{V}_s$ (solid: analytical, $\times$: simulation). All simulations use the following parameter values: $\boldsymbol{f} = \mathbf{180}$ Hz, $\boldsymbol{V}_o = \mathbf{14.5}$ V, $\boldsymbol{V}_d = \mathbf{1}$ V, and $\boldsymbol{L}_s = \mathbf{180}\ \boldsymbol{\mu}$H.

Utilizing $v_{\rm ng}$ from (7) with $i_a > 0, i_c > 0$, and $i_b < 0$

$$v_{\rm sa}(t^+{}_{\rm cross}) \geq \frac{1}{3}V_o + \frac{2}{3}V_d. \tag{32}$$

Here, we approximate the crossing time using the sinusoidal approximation for the current: $\omega t^+{}_{\rm cross} \approx \phi$. Thus

$$V_s \sin(\phi) \geq \frac{1}{3}V_o + \frac{2}{3}V_d. \tag{33}$$

Employing (24), we find the requirement for continuous ac-side conduction

$$V_s \geq \sqrt{\frac{1}{9} + \frac{4}{\pi^2}}(V_o + 2V_d) \approx 0.72(V_o + 2V_d). \tag{34}$$

Equation (34) provides an approximate limiting condition for operation in continuous ac-side conduction. Clearly, this operating mode occurs when the ac line-line source voltages are significantly larger than the rectifier output voltage.

The lower limit value of V_s determined in (34), coupled with the power-factor angle expressed in (24) places a minimum limit on the phase shift between the ac source voltage and currents (and a maximum limit on power factor). Coupled with knowledge of the bridge voltage harmonic content [Fig. 2 and (12)], these limits ensure that the largest harmonic current magnitude (the fifth harmonic) is always less than 10% of the fundamental current. Hence, the approximation for power factor used in (26) is justified.

Section II also considers the case where the ac-side impedance includes a resistive component R_s. For values of R_s much less than the effective resistance R posed by the rectifier, the limit (34) does not change much. Continuous ac-side conduction can also occur for larger values of source resistance R_s. The limiting condition in this case can be derived in a similar manner but is more complex. The resulting requirement that must be checked is (33) where ϕ is now given by (29).

IV. Example Applications

In this section, we present some numerical examples that verify the validity of the models developed in the last two sections. We compare our analytical results with ones obtained from a circuit simulator and with experimental results. We choose parameters that are appropriate for modeling Lundell-type automotive alternators.

First, consider the system given in Fig. 1 with the following parameter values: $V_o = 14.5$ V, $L_s = 180\ \mu$H, $V_d = 1$ V. Comparisons between analytical and simulated results are shown in Fig. 4(a)–(c). Fig. 4(a) shows the average output current $\langle i_o \rangle$ versus the magnitude of the source voltage V_s with the source frequency $f(\omega = 2\pi f)$ fixed at 180 Hz. Fig. 4(b) shows the average output current $\langle i_o \rangle$ versus the source frequency f with the source voltage V_s fixed at 20 V. Fig. 4(c) depicts the power factor k_p versus the source voltage V_s with the source frequency f fixed at 180 Hz. In Fig. 4(a) and (b), analytical results are obtained by the use of (25) while the symbol $(\times)$ represents the results from circuit simulation. The predictions using the classical con-

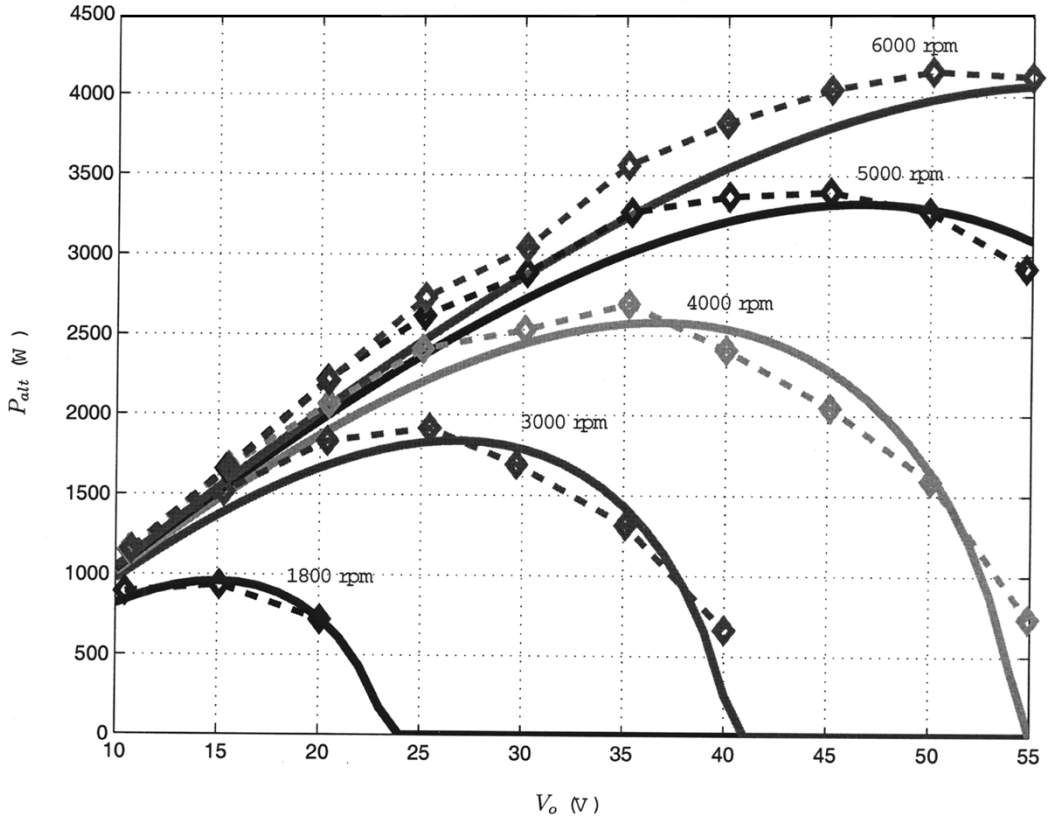

Fig. 5. Alternator output power versus alternator output voltage for several speeds with $\boldsymbol{V_d = 1}$ V, $\boldsymbol{L_s = 135}$ μH, $\boldsymbol{i_f = 3.6}$ A, and $\boldsymbol{k = 9 \times 10^{-3}}$ V/(A$\cdot$ rad/s). Solid and dashed plots correspond to analytical and experimental results, respectively.

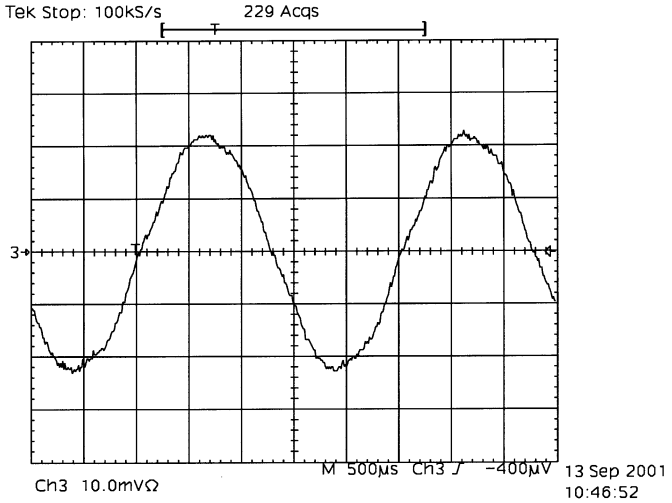

Fig. 6. Measured alternator phase current for 4000 rpm, $\boldsymbol{V_o = 14}$ V, and $\boldsymbol{i_f = 3.6}$ A. Measurement scale is 50 A/div.

stant-current model [1] are shown with a dashed line. In Fig. 4(c), (26) was used to generate the analytical results. As can be seen from these comparisons, there is good agreement between the simulated and analytical results. It can also be seen that the model developed here is much more accurate than the classical constant-current model for the case of a constant-voltage load.

The circuit of Fig. 1 can be utilized as a simplified model of a Lundell alternator [11], [12], allowing the alternator performance to be calculated using the analytical results. Fig. 5 compares the results of the analytical model with the measured behavior of a Lundell alternator operated at constant field current ($i_f = 3.6$ A) across a range of operating conditions. The analytical model uses a synchronous inductance $L_s = 135$ μH and a source voltage magnitude $V_s(= k\omega i_f)$ proportional to speed with proportionality constant $k = 9\times10^{-3}$V/(A$\cdot$ rad/s). Fig. 6 shows the measured phase current of the alternator for a mechanical speed of 4000 rpm (400-Hz electrical frequency), output voltage $V_o = 14$ V, and field current $i_f = 3.6$ A. As can be seen, the analytical model does an excellent job of capturing the alternator behavior despite the substantial simplifications that were employed. The alternator operates in continuous ac-side conduction mode with highly sinusoidal waveforms. We, thus, conclude that the proposed models are accurate and useful for modeling real systems.

V. Conclusion

In this brief, we have presented an analysis of the operating characteristics of three-phase bridge rectifiers with ac-side reactance and constant-voltage loads operating in continuous ac-side conduction mode. Classical models based on constant-current loads are not very accurate for such systems. Analytical expressions are derived for the line and output current characteristics and input power factor. The inclusion of series resistance of phases is also described. We also analyze the boundary conditions for the mode of operation considered. The analytical expressions are compared to computer simulations and experimental results and shown to be quite accurate.

Acknowledgment

The authors would also like to thank J. Rivas of MIT for his valuable comments on the manuscript.

REFERENCES

[1] J. G. Kassakian, M. F. Schlecht, and G. C. Verghese, *Principles of Power Electronics*. Reading, MA: Addison Wesley, 1991.

[2] O. H. Schade, "Analysis of rectifier operation," in *Proc. IRE*, vol. 31, 1943, pp. 341–361.

[3] P. Richman, "Wave factors for rectifiers with capacitor input filters, and other high crest factor loads," *IEEE Trans. Ind. Electron. Contr. Instrum.*, vol. 21, pp. 235–241, Nov. 1974.

[4] A. G. Bogle, "Rectifier circuit performance: Some new approximate formulas," in *Proc. Inst. Electron. Eng.*, vol. 124, 1977, pp. 1127–1134.

[5] A. Lieders, "Single-phase rectifier circuits with CR filters, part 1—Theory," *Electron. Compon. Applicat.*, vol. 1, no. 3, pp. 153–163, 1979.

[6] W. P. Gibbons, "Current and voltage waveform distortion analysis on three-phase "wye" power systems with rectifier loads," *IEEE Trans. Ind. Applicat.*, vol. IA-19, pp. 181–190, Mar./Apr. 1983.

[7] K. S. Hall, "Calculation of rectifier-circuit performance," in *Proc. Inst. Elect, Eng.—Part A*, vol. 127, 1980, pp. 54–60.

[8] J. Schaefer, *Rectifier Circuits: Theory and Design*. New York: Wiley, 1965.

[9] A. W. Kelley and W. F. Yadusky, "Rectifier design for minimum line-current harmonics and maximum power factor," *IEEE Trans. Power Electron.*, vol. 7, pp. 332–341, Apr. 1992.

[10] M. Grotzbach and R. Redmann, "Line current harmonics of VSI-fed adjustable-speed drives," *IEEE Trans. Ind. Applicat.*, vol. 36, pp. 683–690, Mar./Apr. 2000.

[11] D. J. Perreault and V. Caliskan, "A new design for automotive alternators," in *Proc. Int. Congr. Transportation Electronics (Convergence 2000)*, Oct. 2000, SAE Paper 2000-01-C084, pp. 583–594.

[12] D. J. Perreault and V. Caliskan, "Automotive power generation and control," MIT Laboratory for Electromagnetic and Electronic Systems, Cambridge, MA, Tech. Rep. TR-00-003, May 2000.

Lyapunov-Based Control Strategy for Power-Factor Preregulators

Hasan Kömürcügil and Osman Kükrer

***Abstract*—A new control strategy based on Lyapunov's direct method is proposed for power-factor preregulators. It is shown that a globally stable control is possible at the expense of a time-varying reference function for the output voltage. Due to the practical difficulty and complexity in estimating the ripple component on the output voltage, a modified Lyapunov-based control method involving a constant reference for the output voltage is proposed. The method not only ensures stability independent of circuit parameters, but also exhibits excellent transient response to abrupt changes in the load. Moreover, it does not require any estimation technique to estimate the harmonic-ripple component of the output voltage. Computer and experimental results for continuous conduction mode operation are presented to show the applicability of the proposed control method.**

***Index Terms*—Lyapunov's direct method, power-factor preregulator (PFP).**

I. INTRODUCTION

Conventional offline power supplies that incorporate a diode–bridge rectifier and a reservoir capacitor directly connected to the mains draw an input ac current that is far from the ideal sinusoidal wave shape. The harmonic components of this distorted current wave not only lower the input power factor, but also distort the local ac voltage waveform. High input power-factor and near-sinusoidal input ac current can be achieved by utilizing a power-factor preregulator (PFP) in between the diode–bridge rectifier and the reservoir capacitor as shown in Fig. 1. It is shown by many researchers [1]–[10] that the dc–dc boost converter in power-factor-correcting converters is the most frequently utilized topology due to its simplicity and high efficiency.

The hysteresis current control (HCC) presented in [1] offers fast dynamic response, high robustness and simple closed-loop control, but it exhibits some drawbacks that the switching frequency changes with load current resulting in excessive stresses on the switching devices and it requires a precise input current sensing. The control method proposed in [2] requires a complex control circuitry and has no robustness as compared to HCC. It is well known that in these converters the output voltage is composed of a dc value and a harmonic-ripple component at twice the line frequency due to the input power pulsation. The presence of this ripple component on the output voltage not only makes the voltage-loop controller design complicated, but also affects the input current waveform. Therefore, most of the proposed techniques are aimed to cancel the ripple component from the feedback path. But, this requires estimation of the harmonic-ripple component. The adaptive estimator proposed in [3] has the disadvantage that it requires a complex control circuit with a phase-locked loop (PLL). In the control scheme presented in [4], the performance of the controller is sensitive to the estimation of voltage ripple, with the current distortion increasing as the error of estimation increases. In addition to this, it is difficult to select suitable PI gains (as there are two PI regulators), so as to have a stable operation. In most of these studies, the control law proposed is a function of the circuit parameters. In case of parameter variations, this can cause adverse effects on the closed-loop system performance. Furthermore, since the converter exhibits a nonlinear behavior, then it may be stable in the vicinity of the operating point but may not be stable when there is a large load variation. The control methods presented in [7] and [8] are based on a large-signal model of a PFP. Although, these methods are successful in obtaining fast dynamic response for the converter, the one presented in [7] requires a precise estimation of load power.

In this brief, we investigate the applicability of the method presented in [11] to the control of PFPs. It is shown that a robust control is possible at the expense of a time-varying reference function for the output voltage. A modified control law involving a constant reference for the output voltage is then proposed. Computer simulations and experiments are presented to show the effectiveness and applicability of the proposed method for the PFP.

II. PRINCIPLE OF OPERATION AND MODELING

The equations describing the operation of the converter in continuous conduction mode (CCM) can be written as

$$Ldi_r/dt = v_r - \mathbf{d}'v_o \tag{1}$$

$$Cdv_o/dt = \mathbf{d}'i_r - (v_o/R_{\text{load}}) \tag{2}$$

where $\mathbf{d}' = D_o' + \Delta d'$ is the unipolar switching function (duty ratio of the diode D), $0 < \mathbf{d}' < 1$, (D_0' and $\Delta d'$ are the steady-state and the perturbed values of $\mathbf{d}'$, respectively), $v_r = |V_m \sin(\omega t)|$ is the full-wave rectified input voltage. In order to achieve unity power factor, the full-wave rectified input current i_r is required to follow a reference

$$i_r^* = |I_m \sin(\omega t)| \tag{3}$$

Manuscript received April 28, 2000; revised February 6, 2001 and February 24, 2003. This paper was recommended by Associate Editor D. Czarkowski.

H. Kömürcügil is with the Department of Computer Engineering, Eastern Mediterranean University, Mersin 10, Turkey (e-mail: hasan.komurcugil@emu.edu.tr).

O. Kükrer is with the Department of Electrical and Electronic Engineering, Eastern Mediterranean University, Mersin 10, Turkey (e-mail: osman.kukrer@emu.edu.tr).

Digital Object Identifier 10.1109/TCSI.2003.816324